Crystal Structure Determination of the Γ_2 Phase in the Fe-Zn-Al System by Single-Crystal Synchrotron X-ray Diffraction Combined with Scanning Transmission Electron Microscopy

Norihiko L. Okamoto[1,2,*], Haruyuki Inui[1,2], Akira Yasuhara[3], and Shu Yamaguchi

[1]*Department of Materials Science and Engineering, Kyoto University, Kyoto 606-8501, Japan*

[2]*Center for Elements Strategy Initiative for Structure Materials (ESISM), Kyoto University, Kyoto 606-8501, Japan*

[3]*EM Application Group, JEOL Ltd., Akishima, Tokyo, 196-8558, Japan*

[4]*Department of Materials Engineering, University of Tokyo, 7-3-1 Hongo, Tokyo, 113-8656, Japan*

***Corresponding Author Contact Information:**
Norihiko L. Okamoto
Department of Materials Science and Engineering, Kyoto University
Sakyo-ku, Kyoto 606-8501, Japan
Tel: +81-75-753-5481
Fax: +81-75-753-5461
E-mail: okamoto.norihiko.7z@kyoto-u.ac.jp

Abstract

The crystal structure of the Γ_2 phase in the Fe-Zn-Al ternary system has been determined by single-crystal synchrotron X-ray diffraction combined with scanning transmission electron microscopy. The Γ_2 phase possesses the γ'-brass structure with the space group of $F\bar{4}3m$, similarly to the Γ_1 phase in the Fe-Zn binary system. However, the Γ_1 and Γ_2 phases are not isostructural with each other because the constituent cluster types are different when described by the nested cluster model. Moreover, the crystal structure of the Γ_2 phase can be classified into a new type of the γ'-brass structure since it comprises a nested cluster (the Ti_2Ni type with a cluster centre (CC) atom) which does not exist in any of the γ'-brass structures ever reported. The unit cell of the Γ_2 phase contains 32 Fe, 16 Al and 348 Zn atoms so that the compound is expressed with the chemical formula of $Fe_8Zn_{87}Al_4$, and comprises Fe-centred Zn_{12} and Zn_9Al_3 icosahedra, Zn-centred Zn_{10} polyhedra and tetrapods consisting of split sites of Zn atoms with partial occupancies.

Keywords: Intermetallic phase; Galvannealed steel; Phase diagram; Coordination polyhedra; Icosahedron; Focused ion beam (FIB)

1. Introduction

The coating layer of hot-dipped galvannealed (GA) steels, which have widely been used in the automobile industry [1], usually consists of five intermetallic compounds, Γ (Fe_3Zn_{10}), Γ_1 ($Fe_{11}Zn_{40}$), δ_{1k} ($FeZn_7$), δ_{1p} ($Fe_{13}Zn_{126}$) and ζ ($FeZn_{13}$) phases in decreasing order of Fe content [2-8]. When GA steels are deformed under severe conditions such as press-forming operations, the coating layer occasionally fails by decohesion at the coating/substrate interface (flaking) or by intracoating cracking to form fine particles (powdering). There is an ever-increasing demand for improving the formability of GA steels from both technical and economic aspects. Knowledge on the structural (crystal structure, microstructure and so on) and mechanical (deformation, elastic, fracture and so on) properties for each of the five intermetallic compounds is indispensable to achieve the formability improvement and these properties have been the subjects of many studies in the last decades [6, 7, 9-17]. GA steels are produced by immersing steel strips into a bath of molten zinc followed by heat-treatment to alloy the zinc coating with the substrate iron through thermal diffusion. Aluminium is usually added in the molten zinc bath in practical industrial operations for giving the better lustre of the coating, for reducing the oxidation rate of the zinc bath, and also for controlling the layer thickness of the intermetallic compounds through the adjustment of the incubation period of the Fe-Zn reaction [18]. The thermodynamics and crystallography of relevant phases in the Fe-Zn-Al ternary system are therefore very important as in the case of those in the Fe-Zn binary system and have thus been intensively investigated for a several decades [1, 4, 18-24]. Koster and Godecke [19] performed the first systematic study on phase equilibria in the Fe-Zn-Al system and reported that the only ternary compound, $FeZn_8Al$, exists at 450°C in the ternary system. Then, Perrot et al. [23] re-investigated the ternary phase diagram in more detail and reported that a ternary phase (Γ_2) with a mean composition of Zn-6 at.%Al-8 at.%Fe is in equilibrium with the binary δ_1 (δ_{1k}/δ_{1p}) phase at 450°C. They concluded that the ternary Γ_2 phase is

isostructural with the binary Γ_1 phase from the fact that X-ray diffraction (XRD) patterns from these two phases were identical with each other, even though the atomic coordinates for Al were not specified. However, there remain some questions as to whether or not the ternary Γ_2 phase is isostructural with the binary Γ_1 phase, since they failed to observe a continuous solid-solution between the Γ_2 and Γ_1 phases, which would likely occur when judged from a very small difference (~0.4 %) in their lattice constants.

Recently, we have refined the crystal structure for the δ_{1p} phase ($Fe_{13}Zn_{126}$) in the Fe-Zn system by synchrotron XRD combined with scanning transmission electron microscopy (STEM), demonstrating the power of the combined technique in crystal structure refinement particularly for complex crystal structures [7]. The power of the combined technique is that any discrepancies between the real structure and structural model deduced from XRD refinement can directly be detected through direct observations of individual atomic columns with spherical-aberration (Cs) corrected STEM imaging of ultra-high-resolution (spatial resolution: $\leq$ 0.8 Å) and vice versa. As a result of analysis based on the combined technique, we have elucidated that the crystal structure of the δ_{1p} phase comprises coordination polyhedra including normal Zn_{12} icosahedra, disordered Zn_{12} icosahedra and Zn_{16} icosioctahedra with Fe atoms exclusively allocated to the centre of icosahedra [7], completely modifying the model reported by Belin et al. [25].

In the present study, we determine the crystal structure of the Γ_2 phase by synchrotron XRD combined with ultra-high-resolution Cs-corrected STEM that permits direct observation of individual atomic columns, in order to see (1) if the Γ_2 phase in the Fe-Zn-Al ternary system also crystallizes into one of the γ'-brass structures that are sometimes described by the nested cluster model [26, 27] as described in the next section and (2) if the Γ_2 phase in the Fe-Zn-Al ternary system is isostructural with the Γ_1 phase in the Fe-Zn binary system.

2. Description of the γ'-brass structures by the nested cluster model

The Γ_1 phase ($Fe_{11}Zn_{40}$) in the Fe-Zn binary system crystallizes into the γ'-brass structure [28], whose crystal structure is usually described as a 2×2×2 ordered superstructure based on the γ-brass structure with a doubled lattice constant of the cubic unit cell so that the unit cell volume for the γ'-brass structure is eight times that for the γ-brass structure [26, 27, 29]. The Γ phase (Fe_3Zn_{10}) in the Fe-Zn system is known to crystallize into the γ-brass structure (prototype: Cu_5Zn_8, $D8_2$ in the Strukturbericht notation, space group $I\bar{4}3m$, Pearson symbol *cI*52) [25, 30-32]. The cubic unit cell of the γ-brass structure is sometimes described by the nested cluster model, in which a 26-atom nested cluster (Fig. 1(a)) is allocated to every lattice point of the body-centred cubic lattice (Fig. 2(a)) [8, 25]. The 26-atom cluster consists of inner tetrahedron (IT), outer tetrahedron (OT), octahedron (OH), and cuboctahedron (CO), which are nested inside one another, as shown in Fig. 1(a). The γ'-brass structure is built by stacking two unit cells of the γ-brass structure respectively along three cubic axes and by allocating some nested atom clusters to the corresponding crystallographic special positions [26, 27]. Nested atom clusters in the γ'-brass structure can be not only the 26-atom cluster (γ-brass type) described above but also some different types of atom clusters based on the 26-atom cluster, as listed below.

(i) γ-brass type (26 atoms): IT+OT+OH+CO (Fig. 1(a))

(ii) Ti_2Ni type (22 atoms): OT+OH+CO (Fig. 1(b))

(iii) α-Mn type (29 atoms): CC+IT+OT+TT+CO (Fig. 1(c))

(iv) b.c.c. type (27 atoms) CC+ IT+OT+OH+CO (Fig. 1(d)),

where CC and TT denote the cluster centre and truncated tetrahedron, respectively [26, 27]. Since the unit cell volume of the γ'-brass structure is eight times that of the γ-brass structure, the number of nested atom clusters allocated to the unit cell of the γ'-brass structure is 16. These clusters are allocated to four special positions in the face-centred cubic lattice of the

γ'-brass structure with the space group $F\bar{4}3m$; Z(0,0,0), Q(1/4,1/4,1/4), H(1/2,1/2,1/2), T(3/4,3/4,3/4)[1] [26, 33]. The Z position is always occupied by the regular γ-brass type cluster in all the γ'-brass compounds so far reported. Other different types of atom clusters (as well as the γ-brass type cluster) are allocated to other positions with and without some modifications such as addition/elimination of the CC atom and IT. Many different types of the γ'-brass structure can be generated depending on the combination of the nested cluster types with and without modification and their allocation. Indeed, eight different types of the γ'-brass structure have been reported to exist as tabulated in Table 1 [26]. The Γ_1 phase in the Fe-Zn binary system ($Fe_{11}Zn_{40}$) is classified into the $Mg_{44}Rh_7$ type, in which the regular γ-brass type clusters reside at the Z and T positions, Ti_2Ni type cluster at the Q position, and the α-Mn type cluster without the CC atom at the H position (Fig. 2(b) and Tables 1 and 4) [26, 28].

3. Experimental procedures

Large (~20 mm) single crystals of the Γ_2 phase of high quality for single-crystal XRD were obtained from the molten zinc-aluminium bath in the GA steel fabrication process. The average chemical composition evaluated on several different crystals by energy dispersive X-ray spectroscopy (EDS) in a scanning electron microscope was Zn-8.1 at.%Fe-4.3 at.%Al. A cylindrical specimen with approximately 28 μm in diameter and 20 μm in length was machined from one of the single crystals with a JEOL JIB-4000 focused ion beam (FIB) apparatus at an operating voltage of 30 kV. Synchrotron XRD experiments were carried out at 298 K with a large cylindrical image-plate (IP) camera installed at the BL02B1 of SPring-8. The large IP camera enables to obtain high statistic data. The wavelength of the incident X-ray used was 0.35450 Å (35.00 keV). The crystal structure was solved by direct methods

[1] The Z, Q, H, and T positions are the 4*a*, 4*c*, 4*b*, and 4*d* Wyckoff sites in the space group $F\bar{4}3m$. Z: zero, Q: quarter, H: half, T: three-quarters.

(*SIR97*) [34] and refined by full-matrix least-squares techniques on F^2 (*SHELXL-97*) [35]. All calculations were performed with the *WinGX* crystallographic software package [36, 37]. Ultra-high-resolution (spatial resolution: $\leq$ 0.8 Å) STEM imaging was made with a Cs-corrected JEOL JEM-ARM200F STEM operated at 200 kV. The probe convergence angle and the inner/outer detector angles for high-angle annular dark-field (HAADF) imaging were 22 and 90/370 mrad, respectively. Elemental mapping at atomic resolution was performed by EDS in the STEM. STEM image simulations were performed with the *WinHREM* software package [38].

4. Results

4.1. STEM imaging

Fig. 3(a) indicates an experimental high-resolution HAADF-STEM image of the Γ_2 phase taken along the $[1\bar{1}0]$ zone-axis orientation. Many atomic columns are resolved separately from other columns in spite of the fairly complex crystal structure. Bright spots are observed to arrange in pseudo-hexagonal rings (as indicated by dashed hexagons in Fig. 3(a)) surrounding the brightest spot in the centre. A HAADF-STEM image calculated for the Γ_1 phase in the Fe-Zn system with the atomic coordinates given by Koster and Schoone [28] is shown in Fig. 3(b). Although image calculation can reproduce many details of the experimental image, some parts of the experimental image of Fig. 3(a) cannot be well reproduced by image calculation, as indicated by solid and dashed circles in Figs. 3(a) and (b). The intensity of these encircled portions in the experimental image of Fig. 3(a) is considerably weak when compared to that in the calculated image of Fig. 3(b). This clearly indicates that the actual crystal structure of the Γ_2 phase in the Fe-Zn-Al system is different from that of the Γ_1 phase in the Fe-Zn system refined by Koster and Schoone [28]. When referring to the crystal structure of the Γ_1 phase given by Koster and Schoone [28] (Fig. 3(c)),

the portions indicated by solid circles correspond to the Fe3 sites (16*e* sites in the Wyckoff notation) while those indicated by dashed circles correspond to the mixed Fe/Zn2 sites (16*e*). Since the intensity of atomic columns in the atomic-resolution HAADF-STEM image is approximately proportional to the square of the average atomic number [39], the average atomic number of the corresponding atomic columns in the actual crystal structure of the Γ_2 phase in the Fe-Zn-Al system must be smaller than that expected from the crystal structure of the Γ_1 phase given by Koster and Schoone [28]. These atomic columns may contain either a lighter element (Al in the present case) or vacancies with partial or full occupancy.

EDS elemental maps for Fe and Al are shown in Figs. 4(b) and (c), together with the HAADF-STEM reference image of the same area (Fig. 4(a)). Areas A and B enriched with Fe are noted in Fig. 4(b). The area A corresponds to the Fe2, Zn5 and Zn6 sites (16*e*, 48*h* and 24*g*) of the Γ_1 phase in the Fe-Zn system, where the brightest spot is observed in the HAADF-STEM image. The area B, on the other hand, corresponds to the Fe2, Fe/Zn3, Zn1, and Zn4 sites (16*e*, 16*e*, 48*h* and 48*h*) of the Γ_1 phase in the Fe-Zn system, having a boomerang shape intensity in the upper two sides of the outer hexagonal ring. Areas enriched with Al are found at the corner and centre of the projected half unit cell (dashed frame in Fig. 4(c)), although the enrichment is not significantly marked. These positions correspond to the origin and face-centre positions of the cubic unit cell. Since the Fe/Zn2 site is the closest to the unit cell origin in the Γ_1 phase (Table 3 and Figs. 2(b) and 4(d)), Al atoms in the Γ_2 phase are considered to occupy a crystallographic site corresponding to the Fe/Zn2 site in the Γ_1 phase. This may result in the weaker intensity of the portions indicated by dashed circles in the HAADF-STEM image of Fig. 3(a).

4.2. Single-crystal synchrotron X-ray diffraction

The details of the single-crystal XRD are given in Table 2. The space group $F\bar{4}3m$ was assigned to the Γ_2 phase in the Fe-Zn-Al system, similarly to the Γ_1 phase in the Fe-Zn system [28]. Neither additional reflections nor streaks were observed even when the image-plate was overexposed. In the structure determination, we employed the following procedures. 13 crystallographic sites were first found in the initial structural solution using the *SIR97* software [34]. When all atoms were assumed to be Zn with full occupancy, three of the 13 atomic sites exhibited extraordinarily large isotropic thermal parameters. The Zn atoms in the three sites were thus replaced by Fe (Fe1 and Fe2 sites) or Al atoms (Al1 site), resulting in much smaller residual (*R*) factors. The remaining 10 atomic sites were considered to be Zn because they exhibited ordinary isotropic thermal parameters (Zn1-Zn10 sites). Since a large positive residual density was (~50 eÅ^{-3}) still found in the 4*b* sites (1/2,1/2,1/2), an additional Zn site (Zn11) was assigned as the 4*b* site with partial occupancy. Nevertheless, large positive residual density peaks were found in the vicinity (1.9 Å) of the Zn11 site (4*b*). Therefore, five more additional Zn sites (Zn12-Zn16) were assigned as the 16*e* sites around the Zn11 site. These Zn sites (Zn11-Zn16) are regarded as split sites with partial occupancies when judged from the very short distance among them (~0.3−0.9 Å) and form a tetrapod centred at the 4*b* site. This kind of positional disorder accompanied by partial occupancies is commonly observed in many Zn-rich compounds [40-43]. Although the occupancies for the first 13 sites (Fe1/Fe2/Al1/Zn1-Zn10) were allowed to vary, all of them virtually converged to be unity, indicating the absence of vacancies except for the six split sites (Zn11-Zn16). Subsequently, the occupancies for the Zn11-Zn16 sites were allowed to vary. The sum of the occupancies for the split sites at the 16*e* sites (Zn12-Zn16) converged to almost unity (1.026) (*i.e.* ~16 Zn atoms per unit cell) while the occupancy for the Zn11 site (4*b*) converged to 0.194 (*i.e.* nearly one Zn atom per unit cell). Thus, on average 4.3 Zn atoms are distributed

over each of the tetrapods centred at the 4*b* site. Further refinement by allowing mixed occupation between Zn/Fe and Al for the first 13 sites revealed that all the sites are virtually exclusively occupied by each of these species. Finally, anisotropic thermal parameters for the first 13 sites were refined.

Table 3 gives the atomic coordinates and isotropic thermal parameters refined in the present study for the Γ_2 phase together with the atomic coordinates for the Γ_1 phase reported by Koster and Schoone [28]. The number (19) of crystallographic sites for the Γ_2 phase is larger than that (14) for the Γ_1 phase. This is because the Zn8 site in the Γ_1 phase is split into five split sites (Zn12−Zn16) in the Γ_2 phase and the 4*b* and 4*d* sites occupied by Zn atoms (Zn11 and Zn1, respectively) in the Γ_2 phase are vacant in the Γ_1 phase. On the other hand, the 16*e* sites (Fe3) in the Γ_1 phase are vacant in the Γ_2 phase. In addition, Al atoms (Al1) in the Γ_2 phase exclusively occupy the 16*e* sites corresponding to the Fe/Zn2 sites in the Γ_1 phase. These are consistent with the results of our Cs-corrected STEM observations (Fig. 3(a)–(c)) that the atomic sites corresponding to the Fe3 and Fe/Zn2 sites in the Γ_1 phase are occupied either by lighter Al atoms or by vacancies with partial or full occupancy, as well as with the results of EDS analysis (Fig. 4) that Al atoms in the Γ_2 phase occupy a site corresponding to the Fe/Zn2 site in the Γ_1 phase. The corresponding atomic coordinates for the sites commonly occupied in the Γ_1 and Γ_2 phases are virtually identical with each other, as shown in Table 3.

The unit cell of the Γ_2 phase contains 396 atoms (Pearson symbol *cF*396), of which 32 are Fe atoms, 16 Al atoms, and 348 Zn atoms[2], on the assumption that four Zn atoms form a tetrahedron centred at the 4*b* site with full occupancy (instead of 4.3 Zn atoms being allocated to the Zn11 site (4*b*) and the Zn12-Zn16 sites (16*e*) with partial occupancies). When

[2] Exactly speaking, 349.24 Zn atoms are counted per unit cell. The fractional number of Zn atoms is due to the partial occupancies in the Zn11−Zn16 sites.

referring to the fact that the unit cell contains four chemical formulae because of the face-centred lattice, the Γ_2 phase is formulated to be $Fe_8Zn_{87}Al_4$, instead of $FeZn_8Al$ as previously described by Koster and Godecke [19]. The composition derived from the present structure refinement (Zn-8.1 at.%Fe-4.0 at.%Al) is in good agreement with that estimated by EDS analysis (Zn-8.1 at.%Fe-4.3 at.%Al). Further details of the crystal structure investigation can be obtained from the Fachinformationszentrum Karlsruhe, 76344 Eggenstein-Leopoldshafen (Germany; fax: (+49) 7247-808-666; e-mail: crysdata@fiz-karlsruhe.de) on quoting the depository number CSD-429224.

4.3. Comparison of X-ray diffraction data with Cs-corrected STEM images

Fig. 3(d) shows a HAADF-STEM image calculated based on the structural model of the Γ_2 phase obtained by single-crystal XRD in the present study (Figs. 3(e) and 4(e)). The calculated image of Fig. 3(d) is in good agreement with the corresponding experimental images (Fig. 3(a)), as the intensity of the encircled portions in both the experimental and calculated images is considerably weak. The EDS elemental maps for Fe and Al (Figs. 4(b) and (c)) are also in good agreement with the structural model of the Γ_2 phase because the portions enriched with Fe correspond to the Fe1 and Fe2 sites (Figs. 4(b) and (e)) while those enriched with Al correspond to the Al1 site (Figs. 4(c) and (e)). All these results support the validity of the structural model of the Γ_2 phase refined in the present study.

5. Discussion

5.1. Structural description by the nested cluster model: a new type of the γ′-brass structure

Although the same space group $F\bar{4}3m$ is assigned to both the Γ_2 phase in the Fe-Zn-Al system and the Γ_1 phase in the Fe-Zn system ($Fe_{11}Zn_{40}$) [28], their crystal structures are

different from each other when the crystal structures are described by the nested cluster model [26, 27], as seen in Tables 1 and 4. The crystal structure of the Γ_2 phase in the Fe-Zn-Al system can be regarded as one of the γ'-brass structures as the Γ_1 phase in the Fe-Zn system is, since the Γ_2 phase can be described as comprising a regular γ-brass type cluster (Al1/Fe1/Zn5/Zn7) at the Z position, a regular Ti_2Ni type cluster (Fe2/Zn3/Zn8) at the Q position, an α-Mn type cluster with split sites (Zn11/Zn12-Zn16/Zn10/Zn6) at the H position, and a Ti_2Ni type cluster with an additional CC atom (Zn1/Zn2/Zn4/Zn9) at the T position (Fig. 5). In the Γ_1 phase in the Fe-Zn system, on the other hand, the Ti_2Ni type cluster with an additional CC atom is replaced by a γ-brass type cluster at the T position, and the α-Mn type cluster with split sites is replaced by that without an additional CC atom at the H position (Fig. 2(b)) [26, 28]. This clearly indicates that the Γ_1 phase in the Fe-Zn system and the Γ_2 phase in the Fe-Zn-Al system crystallize into different types of the γ'-brass structures and that they are not isostructural with each other although the same space group is assigned. This is contrary to the previous literature that the ternary Γ_2 phase is isostructural with the binary Γ_1 phase from XRD analysis [23]. The fact that the Γ_1 phase in the Fe-Zn system and the Γ_2 phase in the Fe-Zn-Al are not isostructural with each other is consistent with the absence of a continuous solid-solution between the Γ_2 and Γ_1 phases [23].

Among the eight different types of the γ'-brass structure reported by Berger et al. [26], the $Mg_{44}Rh_7$ and Na_6Tl types comprise almost the same nested clusters (Table 1). The nested clusters at the Z, Q and T positions (regular γ-brass, Ti_2Ni, and regular γ-brass types, respectively) are identical with each other, but the nested cluster at the H position is of the α-Mn type for the γ'-brass structure of the Na_6Tl-type (Fig. 1(c)) while it is of the α-Mn type without CC atom for the γ'-brass structure of the $Mg_{44}Rh_7$ type (Fig. 1(f)). The structural change caused by the elimination of the CC atom in the nested cluster of the α-Mn type is very significant being much more than the introduction of a vacancy in the CC site. In the

absence of the CC atom, the distance between the OT sites (OT-OT) in the nested cluster of the α-Mn type decreases as much as 29%[3], when compared to the corresponding distance in the nested cluster of the 'regular' α-Mn type with CC atom. Moreover, the coordination numbers of the OT and TT sites decrease respectively from 14 and 13 to 12. As is the case for the γ'-brass structures of the $Mg_{44}Rh_7$ and Na_6Tl types, the present Γ_2 phase ($Fe_8Zn_{87}Al_4$) and the Mg_6Pd type also comprise almost the same nested clusters (Table 1). The nested clusters at the Z, Q and H positions (regular γ-brass, Ti_2Ni, and α-Mn types, respectively) are identical with each other, but the nested cluster at the T position is of the Ti_2Ni type for the γ'-brass structure of the Mg_6Pd -type (Fig. 1(b)) while it is of the Ti_2Ni type with CC atom for the γ'-brass structure of the Γ_2 phase (Fig. 1(e)). A drastic structural change occurs in the nested cluster of the Ti_2Ni type by the addition of the CC atom, as in the case of the structural change in the nested cluster of the α-Mn type by the elimination of the CC atom. In the presence of the CC atom, the distance between the OH sites (OH-OH) is increased by 32%[3]. As a result, the OH sites, which are allocated within the cuboctahedron consisting of the CO atoms in the 'regular' Ti_2Ni type cluster (Fig. 1(b)), are protruded outside the cuboctahedron in the Ti_2Ni type cluster with CC atom (Fig. 1(e)). Moreover, the coordination number of the OT site increases from 9 to 10 whereas that of the OH site decreases from 14 to 11 due to the extension of the OH-OH atomic distance. The structural change caused by the addition of the CC atom in the Ti_2Ni type cluster is thus much more than the introduction of an interstitial atom in the CC site. As the $Mg_{44}Rh_7$ and Na_6Tl types are classified into two different types of the γ'-brass structure for the difference in the nested cluster of the α-Mn type (without or with the CC atom) at the H position, the present Γ_2 phase ($Fe_8Zn_{87}Al_4$) and the Mg_6Pd type should be classified into different types of the γ'-brass structure for the difference in the nested

[3] Relative change in the atomic distance is calculated with the corresponding fractional atomic coordinates without taking the magnitude of the lattice constants into account for the ease of comparison.

cluster of the Ti_2Ni type (with or without the CC atom) at the T position. Of importance to note here is that the nested cluster of the Ti_2Ni type with CC atom observed in the present Γ_2 phase ($Fe_8Zn_{87}Al_4$) has never been found in any of the eight types of the γ'-brass structure classified by Berger et al. [26], as shown in Table 1. This clearly indicates that the crystal structure of the present Γ_2 phase is a new type of the γ'-brass structure, which can be counted as the ninth type.

5.2. Structural description by the coordination polyhedra model

The nested cluster model is usually used to describe the crystal structures of the γ'-brass structures [26, 27], as Koster and Schoone [28], who first determined the crystal structure of the Γ_1 phase in the Fe-Zn binary system, did so in the crystal structure description. If crystal structures are complicated considerably as in the γ'-brass structures, however, the crystal structure description based on the packing of coordination polyhedra can sometimes be very helpful for the intuitive understanding of these crystal structures. In the Γ phase with the γ-brass structure, for example, four Fe-centred icosahedra are connected with one another by face-sharing to form a large tetrahedron as shown in Fig. 6 [25]. The vertices of the shared triangle faces are occupied by Fe and Zn atoms to form a $(Fe,Zn)_4$ tetrahedral core. This tetrahedral core corresponds to the IT site whereas the four centred Fe atoms correspond to the OT site in the nested cluster model (see Fig. 2(a)). The vertices of the Fe-centred icosahedra other than those of the tetrahedral core correspond to the OH and CO sites in the nested cluster model (Fig. 6).

We describe the crystal structure of the Γ_2 phase with the coordination polyhedra model below (Fig. 7(a)). The crystal structure of the Γ_2 phase in the Fe-Zn-Al system can be considered to consist of three kinds of agglomerated polyhedra (Figs. 7(b)-(d)) and one tetrapod accompanied by positional disorder of Zn atoms in the 4*b* and 16*e* sites (Fig. 7(e)).

The Fe1 and Fe2 atoms reside at the centre of Zn_9Al_3 and Zn_{12} icosahedra, respectively, as shown in Figs. 7(b) and (c). Four Fe1-centred Zn_9Al_3 icosahedra are connected with one another by face-sharing to form a large tetrahedron with an Al_4 tetrahedral core just as in the case of the Γ phase. On the other hand, four Fe2-centred Zn_{12} icosahedra are connected with one another by sharing vertices at the Zn3 sites. Furthermore, the Fe1- and Fe2-centred icosahedra are connected with each other by sharing vertices at the Zn8 sites. The third agglomerated polyhedra consist of four Zn2-centred Zn_{10} polyhedra, which are fairly distorted, possessing 16 triangle faces, and connected with one another by edge-sharing (Fig. 7(d)). The Zn1 (CC) site resides at the centre of the third agglomerated polyhedra. The Zn2-centred Zn_{10} polyhedra and Fe1-centred icosahedra are connected with each other by sharing vertices at the Zn7 sites. In the remaining space free from the above three kinds of agglomerated polyhedra exists the tetrapod consisting of the split sites with partial occupancies (Zn11-Zn16) (Fig. 7(e)).

On the other hand, the crystal structure of the Γ_1 phase in the Fe-Zn system is described by the coordination polyhedra model as shown in Fig. 7(f). The crystal structure consists of three kinds of agglomerated polyhedra (Figs. 7(g)-(i)) and one Zn_4 tetrahedron (Fig. 7(j)). Four Fe/Zn2-centred icosahedra are connected with one another by face-sharing to form a large tetrahedron as shown in Fig. 7(g). Four Fe2-centred Zn_{12} icosahedra are connected with one another by sharing vertices (Fig. 7(h)). These two agglomerated polyhedra are basically the same as those in the Γ_2 phase (Figs. 7(b) and (c)). On the other hand, the third agglomerated polyhedra consist of six Fe1-centred icosahedra connected with one another by face-sharing to form a large octahedron as shown in Fig. 7(i). Thus, the third agglomerated polyhedra in the Γ_1 phase are totally different from those in the Γ_2 phase (Fig. 7(d)). These three agglomerated polyhedra are connected with one another by sharing vertices. In the remaining space free from the above three kinds of agglomerated polyhedra

exists a Zn_4 tetrahedron consisting of the Zn8 atoms (Fig. 7(j)) instead of the tetrapod observed in the Γ_2 phase (Fig. 7(e)). Therefore, it is again evident that the Γ_1 and Γ_2 phases are not isostructural with each other also when described by the cordination polyhedra model.

The fact that Fe atoms preferentially occupy the centre of Zn_{12} and Zn_9Al_3 icosahedra in the Γ_2 phase indicates that the atomic bonding is stronger for the Fe-(Zn,Al) bond than for the Zn-Zn bond. This is evident from the shorter average bonding distances for the Fe-(Zn,Al) bond (2.607 Å) than those for the Zn-Zn bond (2.745 Å), as seen in the histogram of Fig. 8, in which the bonding distances for the Fe-(Zn,Al), Al-(Fe,Zn,Al), and Zn-Zn bonds (only for those shorter than 3.1 Å) in the Γ_2 phase are plotted. The tendency that the average bonding distance for the Fe-Zn bond is shorter than that for the Zn-Zn bond is also observed for the Γ, δ_{1p} and ζ phases in the Fe-Zn system [7, 25, 44].

6. Conclusions

(1) The crystal structure of the Γ_2 phase in the Fe-Zn-Al ternary system has been determined by single-crystal synchrotron XRD combined with Cs-corrected STEM. The Γ_2 phase possesses the γ'-brass structure with the space group of $F\bar{4}3m$ with the unit cell of a 2×2×2 ordered superstructure of the γ-brass structure, similarly to the Γ_1 phase in the Fe-Zn binary system. The unit cell contains 396 atoms (Pearson symbol *cF*396), of which 32 are Fe atoms, 16 Al atoms and 348 Zn atoms. The Γ_2 phase is formulated to be $Fe_8Zn_{87}Al_4$, instead of $FeZn_8Al$ as previously reported.

(2) The Γ_2 phase can be described by the nested cluster model to be one of the γ'-brass structures comprising a regular γ-brass type cluster at the Z position, a regular Ti_2Ni type cluster at the Q position, an α-Mn type cluster with split sites at the H position, and a Ti_2Ni type cluster with an additional CC atom at the T position. In contrast to the

previous report, the Γ_1 and Γ_2 phases are not isostructural with each other because the constituent cluster types are different when described by the nested cluster model.

(3) The crystal structure of the Γ_2 phase in the Fe-Zn-Al system is a new type of the γ'-brass structure, which has never been reported before, in view of the constituent cluster types in the nested cluster model. In particular, the Ti_2Ni type with CC atom observed at the T position in the Γ_2 phase has never been found in any of the eight types of the γ'-brass structures classified by Berger et al.

(4) The crystal structure of the Γ_2 phase can also be described by the coordination polyhedra model to be packed with Fe-centred Zn_{12} and Zn_9Al_3 icosahedra, Zn-centred Zn_{10} polyhedra and tetrapods consisting of split sites of Zn atoms with partial occupancies. The Γ_1 and Γ_2 phases are not isostructural with each other also when described by the cordination polyhedra model in terms of the constituent agglomerated polyhedra.

Acknowledgements

This work was supported by JSPS KAKENHI grant numbers 24246113 and 25709066, and the Elements Strategy Initiative for Structural Materials (ESISM) from the Ministry of Education, Culture, Sports, Science and Technology (MEXT) of Japan, and in part by Advanced Low Carbon Technology Research and Development Program (ALCA) from the Japan Science and Technology Agency (JST). This work was also supported by Research Promotion Grant from ISIJ and Grants for Technical Research from JFE 21st Century Foundation. The synchrotron radiation experiments were performed at the BL02B1 of SPring-8 with the approval of the Japan Synchrotron Radiation Research Institute (JASRI) (Proposal Nos. 2012B1145, 2013A1394, and 2014B1228). We wish to thank Dr. K. Sugimoto and Dr. N. Yasuda for their assistance at the BL02B1 of SPring-8.

References

[1] A.R. Marder, The metallurgy of zinc-coated steel, Prog. Mater Sci., 45 (2000) 191-271.
[2] O. Kubaschewski, Iron - Binary Phase Diagrams, Springer-Verlage, Berlin, 1982.
[3] X.P. Su, N.Y. Tang, J.M. Toguri, Thermodynamic evaluation of the Fe-Zn system, J. Alloys Compd., 325 (2001) 129-136.
[4] J. Nakano, D.V. Malakhov, G.R. Purdy, A crystallographically consistent optimization of the Zn-Fe system, Calphad, 29 (2005) 276-288.
[5] R. Kainuma, K. Ishida, Microstructural evolution of intermetallic compound layers formed in Fe/Zn binary diffusion couples, Tetsu to Hagane, 91 (2005) 349-355.
[6] N.L. Okamoto, A. Yasuhara, H. Inui, Order-Disorder Structure of the δ_{1k} Phase in the Fe–Zn System Determined by Scanning Transmission Electron Microscopy, Acta Mater., 81 (2014) 345-357.
[7] N.L. Okamoto, K. Tanaka, A. Yasuhara, H. Inui, Structure refinement of the delta(1p) phase in the Fe-Zn system by single-crystal X-ray diffraction combined with scanning transmission electron microscopy, Acta Crystallogr. B, 70 (2014) 275-282.
[8] P. Villars, Pearson's Handbook: Crystallographic Data for Intermetallic Phases, ASM International, Amsterdam, 1997.
[9] M.F. Shi, G.M. Smith, M. Moore, D.J. Meuleman, Galvannealed coating optimized for coating adhesion through dies., in: G. Krauss, D.K. Matlock (Eds.) Zinc-based steel coating systems: metallurgy and performance, TMS, Warrendale, PA, 1990, pp. 387.
[10] A. Iost, J. Foct, Toughness and Residual-Stresses in Galvanizing Coatings, J. Mater. Sci. Lett., 12 (1993) 1340-1343.
[11] C. Kato, H. Koumura, Y. Uesugi, K. Mochizuki, Influence of Phase Composition on Formability of Galvannealed Steel Sheet, in: A.R. Marder (Ed.) TMS Annual Meeting, The Physical Metallurgy of Zinc Coated Steel, TMS, San Francisco, CA, 1994, pp. 241-249.
[12] M.H. Hong, H. Saka, The mechanical properties and dislocation structure of the Γ intermetallic phase in the Fe-Zn system, Philos. Mag. A, 74 (1996) 509-524.
[13] M.H. Hong, H. Saka, Plasticity and grain boundary structure of δ_{1k} and δ_{1p} intermetallic phases in the Fe-Zn system, Acta Mater., 45 (1997) 4225-4230.
[14] M.H. Hong, H. Saka, Transmission electron microscopy of the Fe-Zn δ_1 intermetallic phase, Scripta Mater., 36 (1997) 1423-1429.
[15] A.T. Alpas, J. Inagaki, Effect of microstructure on fracture mechanisms in galvannealed coatings, ISIJ Int., 40 (2000) 172-181.
[16] N.L. Okamoto, D. Kashioka, M. Inomoto, H. Inui, H. Takebayashi, S. Yamaguchi, Compression deformability of Γ and ζ Fe–Zn intermetallics to mitigate detachment of brittle intermetallic coating of galvannealed steels, Scripta Mater., 69 (2013) 307-310.
[17] N.L. Okamoto, M. Inomoto, H. Adachi, H. Takebayashi, H. Inui, Micropillar compression deformation of single crystals of the intermetallic compound ζ-$FeZn_{13}$, Acta Mater., 65 (2014) 229-239.
[18] J. Mackowiak, N.R. Short, Metallurgy of galvanized coatings, Inter. Metals Rev., 24 (1979) 1.
[19] W. Koster, T. Godecke, Ternary Iron-Aluminium-Zinc System, Z. Metallkd., 61 (1970) 649-658.
[20] Urednice.M, J.S. Kirkaldy, Investigation of Phase Constitution of Fe-Zn-Aluminum at 450 Degrees C, Z. Metallkd., 64 (1973) 419-427.
[21] Z.W. Chen, R.M. Sharp, J.T. Gregory, Fe-Al-Zn Ternary Phase-Diagram at 450-Degrees-C, Mater. Sci. Technol., 6 (1990) 1173-1176.
[22] S. Belisle, V. Lezon, M. Gagne, The solubility of iron in continuous hot-dip galvanized

coatings, J. Phase Equilib., 12 (1991) 259.
[23] P. Perrot, J.C. Tissier, J.Y. Dauphin, Stable and Metastable Equilibria in the Fe-Zn-Al System at 450-Degrees-C, Z. Metallkd., 83 (1992) 786-790.
[24] N.-Y. Tang, Comments on Fe-Al-Zn diagram, J. Phase Equilib., 15 (1994) 237.
[25] C.H.E. Belin, R.C.H. Belin, Synthesis and crystal structure determinations in the Γ and δ phase domains of the Fe-Zn system: Electronic and bonding analysis of $Fe_{13}Zn_{39}$ and $FeZn_{10}$, a subtle deviation from the Hume-Rothery standard?, J. Solid State Chem., 151 (2000) 85-95.
[26] R.F. Berger, S. Lee, J. Johnson, B. Nebgen, F. Sha, J.Q. Xu, The mystery of perpendicular fivefold axes and the fourth dimension in intermetallic structures, Chem. Eur. J., 14 (2008) 3908-3930.
[27] A.A. Pankova, V.A. Blatov, G.D. Ilyushin, D.M. Proserpio, gamma-Brass Polyhedral Core in Intermetallics: The Nanocluster Model, Inorg. Chem., 52 (2013) 13094-13107.
[28] A.S. Koster, J.C. Schoone, Structure of the cubic Fe-Zn phase $Fe_{22}Zn_{78}$, Acta Crystallogr. B, 37 (1981) 1905-1907.
[29] J. Dshemuchadse, D.Y. Jung, W. Steurer, Structural building principles of complex face-centered cubic intermetallics, Acta Crystallogr. B, 67 (2011) 269-292.
[30] A.J. Bradley, J. Thewlis, The structure of gamma-brass., Proc. R. Soc. London, Ser. A, 112 (1926) 678-692.
[31] A. Johansson, H. Ljung, S. Westman, X-ray and Nuetron Diffraction Studies on Γ-Ni, Zn and Γ-Fe,Zn, Acta Chem. Scand., 22 (1968) 2743-2753.
[32] J.K. Brandon, R.Y. Brizard, P.C. Chieh, R.K. Mcmillan, W.B. Pearson, New refinements of gamma-brass type structures Cu_5Zn_8, Cu_5Cd_8 and Fe_3Zn_{10}, Acta Crystallogr. B, 30 (1974) 1412-1417.
[33] T. Hahn, International Tables for Crystallography, Vol. A: Space-group symmetry, 5th ed., Springer, Dordrecht, The Netherlands, 2005.
[34] A. Altomare, M.C. Burla, M. Camalli, G.L. Cascarano, C. Giacovazzo, A. Guagliardi, A.G.G. Moliterni, G. Polidori, R. Spagna, SIR97: a new tool for crystal structure determination and refinement, J. Appl. Crystallogr., 32 (1999) 115-119.
[35] G.M. Sheldrick, A short history of SHELX, Acta Crystallogr. A, 64 (2008) 112-122.
[36] L. Farrugia, WinGX suite for small-molecule single-crystal crystallography, J. Appl. Crystallogr., 32 (1999) 837-838.
[37] L. Farrugia, WinGX and ORTEP for Windows: an update, J. Appl. Crystallogr., 45 (2012) 849-854.
[38] K. Ishizuka, A practical approach for STEM image simulation based on the FFT multislice method, Ultramicroscopy, 90 (2002) 71-83.
[39] S.J. Pennycook, L.A. Boatner, Chemically Sensitive Structure-Imaging with a Scanning-Transmission Electron-Microscope, Nature, 336 (1988) 565-567.
[40] S. Lidin, M. Jacob, A.K. Larsson, (Fe,Ni)Zn6.5, a Superstructure of Gamma-Brass, Acta Crystallogr. C, 50 (1994) 340-342.
[41] S. Thimmaiah, K.W. Richter, S. Lee, B. Harbrecht, gamma(1)-Pt5Zn21 - a reappraisal of a gamma-brass type complex alloy phase, Solid State Sci., 5 (2003) 1309-1317.
[42] W. Hornfeck, S. Thimmaiah, S. Lee, B. Harbrecht, Structure-composition relations for the partly disordered Hume-Rothery phase Ir7+7 delta Zn97-11 delta (0.31 <= delta <= 0.58), Chem. Eur. J., 10 (2004) 4616-4626.
[43] S. Thimmaiah, G.J. Miller, On the Structural Chemistry of gamma-Brasses: Two Different Interpenetrating Networks in Ternary F-Cell Pd-Zn-Al Phases, Chem. Eur. J., 16 (2010) 5461-5471.
[44] R. Belin, M. Tillard, L. Monconduit, Redetermination of the Fe-Zn phase $FeZn_{13}$, Acta Crystallogr. C, 56 (2000) 267-268.

Table 1 Cluster types constituting the eight structure types of the γ'-brass compounds classified according to Berger et al. [26] and the Γ_2 phase ($Fe_8Zn_{87}Al_4$).

	$Li_{21}Si_5$	$Mg_{44}Rh_7$ ($Fe_{11}Zn_{40}$)	$(Fe,Ni)_2Zn_{13}$	Mg_6Pd	Na_6Tl	$Zn_{91}Ir_{11}$	$Li_{13}Na_{29}Ba_{19}$	$Al_{69}Ta_{39}$	Γ_2 phase $Fe_8Zn_{87}Al_4$
Z	γ-brass	γ-brass	γ-brass	γ-brass	γ-brass	γ-brass	γ-brass	γ-brass	γ-brass
Q	γ-brass	Ti_2Ni	Ti_2Ni	Ti_2Ni	Ti_2Ni	Ti_2Ni	α-Mn	α-Mn	Ti_2Ni
H	γ-brass	α-Mn w/o CC	α-Mn	α-Mn	α-Mn	α-Mn + IT	α-Mn	α-Mn	α-Mn
T	γ-brass	γ-brass	b.c.c.	Ti_2Ni	γ-brass	γ-brass	γ-brass	b.c.c.	Ti_2Ni + CC

Table 2 Summary of crystallographic data and structure refinement for the Γ_2 phase.

Crystal data	
Chemical formula	$Fe_8Zn_{87}Al_4$
Crystal system	Cubic
Space group	$F\bar{4}3m$
Z	4
Unit cell dimensions (Å)	a = 18.0374(4)
Cell volume (Å^3)	5868.4
Density (calculated) (Mg/m^3)	7.083
Formula weight	6258.25
Absorption coefficient (mm^{-1})	19.271
Crystal size (mm^3)	0.028 × 0.028 × 0.020
Data collection	
Wavelength (Å)	0.35450
θ range for data collection (degree)	0.98 – 23.18
Index ranges	$-37 \le h \le 40$ $-35 \le k \le 39$ $-35 \le l \le 12$
Reflections collected	12128
Independent reflections	3228
Independent reflections ($I > 2\sigma(I)$)	3168
Completeness to θ= 23.18°	99.7 %
R_{int}	0.0222
Refinement	
Refinement method	Full-matrix least-squares on F^2
Number of reflections used	3228
Number of refined parameters	73
Goodness-of-fit on F^2	1.132
R_1 ($I > 2\sigma(I)$)	0.0203
wR_2 ($I > 2\sigma(I)$)	0.0646
R_1 (all data)	0.0208
wR_2 (all data)	0.0650
Largest diffraction peak and hole (eÅ^{-3})	3.559/ -2.070

Computer programs: *SIR97* [34], *SHELXL97* [35], *WinGX* publication routines [36, 37].

Table 3 Atomic coordinates for the Γ_2 and Γ_1 phases and equivalent isotropic displacement parameters U_{eq} for the Γ_2 phase. U_{eq} is defined as one-third of the trace of the orthogonalized U^{ij} tensor.

Γ_2 phase ($Fe_8Zn_{87}Al_4$)							Γ_1 phase ($Fe_{11}Zn_{40}$)					
Atom	Wyckoff	Occ.	x	y	z	U_{eq} (Å^2)	Atom	Wyckoff	Occ.	x	y	z
Fe1[†]	16*e*	1	0.0829(1)	x	x	0.007(1)	Fe/Zn3	16*e*	1	0.0817	x	x
Fe2[‡]	16*e*	1	0.3498(1)	x	x	0.005(1)	Fe2	16*e*	1	0.3514	x	x
Al1	16*e*	1	0.9469(1)	x	x	0.007(1)	Fe/Zn2	16*e*	1	0.9486	x	x
Zn1	4*d*	1	3/4	3/4	3/4	0.015(1)						
Zn2[¶]	16*e*	1	0.8368(1)	x	x	0.012(1)	Fe/Zn1	16*e*	1	0.8345	x	x
Zn3	24*g*	1	0.1429(1)	3/4	3/4	0.010(1)	Zn6	24*g*	1	0.1440	3/4	3/4
Zn4	24*g*	1	0.9062(1)	3/4	3/4	0.013(1)	Fe1	24*g*	1	0.9115	3/4	3/4
Zn5	24*f*	1	0.8142(1)	0	0	0.017(1)	Zn7	24*f*	1	0.8149	0	0
Zn6	48*h*	1	0.8094(1)	x	0.4800(1)	0.013(1)	Zn2	48*h*	1	0.8078	x	0.4768
Zn7	48*h*	1	0.8434(1)	x	0.9809(1)	0.014(1)	Zn1	48*h*	1	0.8444	x	0.9785
Zn8	48*h*	1	0.8930(1)	x	0.2185(1)	0.012(1)	Zn4	48*h*	1	0.8925	x	0.2169
Zn9	48*h*	1	0.9035(1)	x	0.7173(1)	0.021(1)	Zn3	48*h*	1	0.8995	x	0.7143
Zn10	48*h*	1	0.9514(1)	x	0.3411(1)	0.015(1)	Zn5	48*h*	1	0.9501	x	0.3380
Zn11[#]	4*b*	0.194(7)	1/2	1/2	1/2	0.016(1)						
Zn12[#]	16*e*	0.065(4)	0.5285(3)	x	x	0.018(2)						
Zn13[#]	16*e*	0.051(5)	0.5448(5)	x	x	0.016(2)						
Zn14[#]	16*e*	0.165(7)	0.5597(3)	x	x	0.014(1)	Zn8	16*e*	1	0.5597	x	x
Zn15[#]	16*e*	0.402(8)	0.5708(2)	x	x	0.013(1)						
Zn16[#]	16*e*	0.346(8)	0.5812(1)	x	x	0.014(1)						
							Fe3	16*e*	1	0.2027	x	x

[†]Centre of Zn_9Al_3 icosahedra
[‡]Centre of Zn_{12} icosahedra
[¶]Centre of Zn_{10} polyhedra having 16 triangle faces
[#]Split sites constituting a tetrapod

Table 4 Number of atoms per unit cell and atomic sites for $Fe_8Zn_{87}Al_4$ (Γ_2 phase) and $Fe_{11}Zn_{40}$ (Γ_1 phase) with the γ'-brass structures. The atomic sites are sorted according to the nested cluster model [26, 27].

		$Fe_8Zn_{87}Al_4$ (Present study)	$Fe_{11}Zn_{40}$ [28]
Number of atoms per unit cell		396	408
Z		γ-brass type	γ-brass type
	IT	Al1	Fe/Zn2[¶]
	OT	Fe1	Fe/Zn3[¶]
	OH	Zn5	Zn7
	CO	Zn7	Zn1
Q		Ti_2Ni type	Ti_2Ni type
	OT	Fe2	Fe2
	OH	Zn3	Zn6
	CO	Zn8	Zn4
H		α-Mn type with split sites	α-Mn type w/o CC
	CC	Zn11[†]	-
	OT	Zn12-16[#†]	Zn8
	TT	Zn10	Zn5
	CO	Zn6	Zn2
T		Ti_2Ni type with CC	γ-brass type
	CC	Zn1	-
	IT	-	Fe3
	OT	Zn2	Fe/Zn1[¶]
	OH	Zn4	Fe1
	CO	Zn9	Zn3

[#] Split sites
[†] Partial occupancy
[¶] Mixed occupancy

Figure Legends

Figure 1 (a) γ-brass type (26 atoms), (b) Ti_2Ni type (22 atoms), (c) α-Mn type (29 atoms), (d) b.c.c. type (27 atoms) (e) Ti_2Ni+CC type (23 atoms), and (f) α-Mn type without CC (28 atoms) clusters constituting the γ'-brass structure.

Figure 2 Unit cells of the (a) γ-brass and (b) γ'-brass structures described in the nested cluster model [26, 27]. (a) Unit cell of the γ-brass structure consisting of two γ-brass type (26 atoms) clusters (Fig. 1(a)) residing at the cell corner and body centre [30]. (b) Unit cell of the Γ_1 phase ($Fe_{11}Zn_{40}$) with the γ'-brass structure consisting of two regular γ-brass type clusters residing at the Z and T positions, Ti_2Ni type cluster at the Q position, and the α-Mn type cluster without the CC atoms at the H position [28].

Figure 3 (a) HAADF image taken along the $[1\bar{1}0]$ zone axis with the Cs-corrected STEM. HAADF images calculated with the structural parameters (b) for the Γ_1 phase ($Fe_{11}Zn_{40}$) reported by Koster and Schoone [28] and (d) for the Γ_2 phase ($Fe_8Zn_{87}Al_4$) determined by synchrotron XRD in the present study. The corresponding portion of $[1\bar{1}0]$ projection of the structural models for the (c) Γ_1 and (e) Γ_2 phases.

Figure 4 (a) Reference HAADF-STEM image and elemental maps for (b) Fe and (c) Al, respectively, obtained in the atomic-resolution EDS mapping. The corresponding portion of $[1\bar{1}0]$ projection of the structural models for the (d) Γ_1 and (e) Γ_2 phases.

Figure 5 Unit cell of the Γ_2 phase ($Fe_8Zn_{87}Al_4$) described in the nested cluster model [26, 27]. The γ'-brass structure consists of regular γ-brass type cluster residing at the Z position, Ti_2Ni type cluster at the Q position, α-Mn type cluster with split sites at the H position, and Ti_2Ni type cluster with an additional CC atom at the T position.

Figure 6 Unit cell of the Γ phase in the Fe-Zn system [25].

Figure 7 Unit cells of the (a-e) Γ_2 and (f-j) Γ_1 phases described in the coordination polyhedra model. (b,g) Four icosahedra ($Fe1@Zn_9Al_3$, $Fe/Zn2@(Fe.Zn)_{12}$) connected with one another by face-sharing. (c,h) Four Fe-centred Zn_{12} icosahedra ($Fe@Zn_{12}$) connected with one another by vertex-sharing. (d) Four Zn2-centred Zn_{10} polyhedra connected with one another by edge-sharing. (i) Six Fe1-centred icosahedra connected with one another by face-sharing. (e) Zn tetrapod comprising split sites (Zn11-Zn16) and (j) Zn_4 tetrahedron filling the remained space which is not occupied by the agglomerated polyhedra

Figure 8 Histogram of the bonding distances for the Fe-(Zn,Al), Al-(Fe,Zn,Al), and Zn-Zn bonds (shorter than 3.1 Å) in the Γ_2 phase ($Fe_8Zn_{87}Al_4$).

Graphical Abstract (for review)

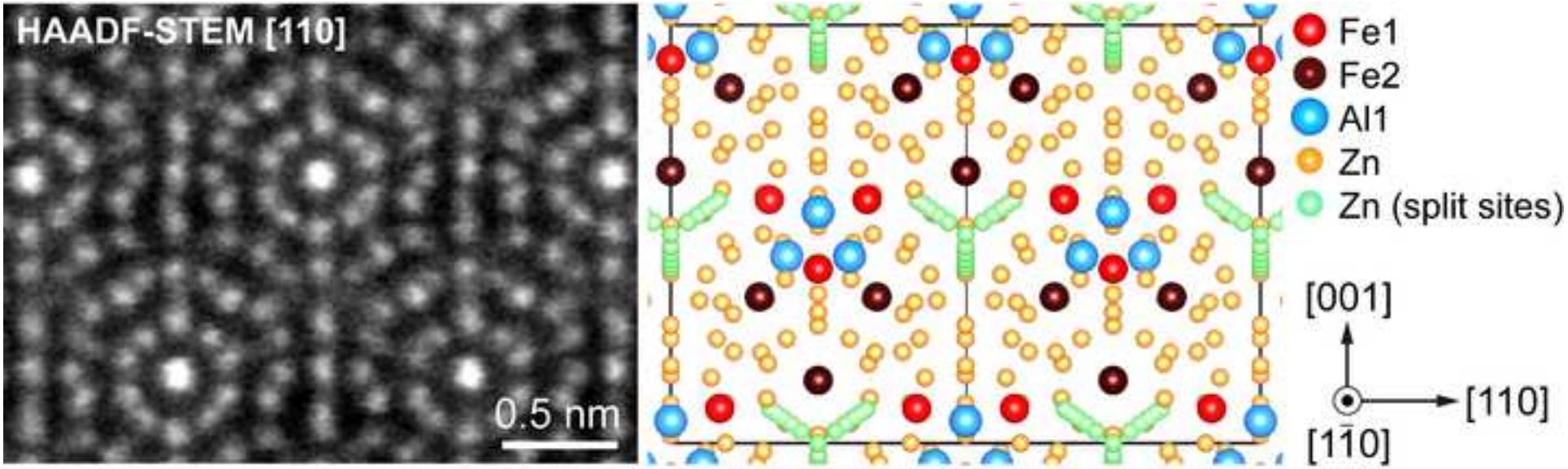

γ'-brass structures: Γ_2 (Fe-Zn-Al) ≠ Γ_1 (Fe-Zn)

No solid-solution between Γ_2 and Γ_1

Highlights (85 characters, 3-5 bullets)

The crystal structure of the Γ_2 phase in the Fe-Zn-Al system has been determined.
The Γ_2 phase possesses the γ'-brass structure with the space group of $F\bar{4}3m$.
The Γ_2 phase is not isostructural with the Γ_1 phase in the Fe-Zn binary system.
The Γ_2 phase belongs to a new (ninth) type of the γ'-brass structure.
The Γ_2 phase is expressed with the chemical formula of $Fe_8Zn_{87}Al_4$.

fig1.tif
Click here to download high resolution image

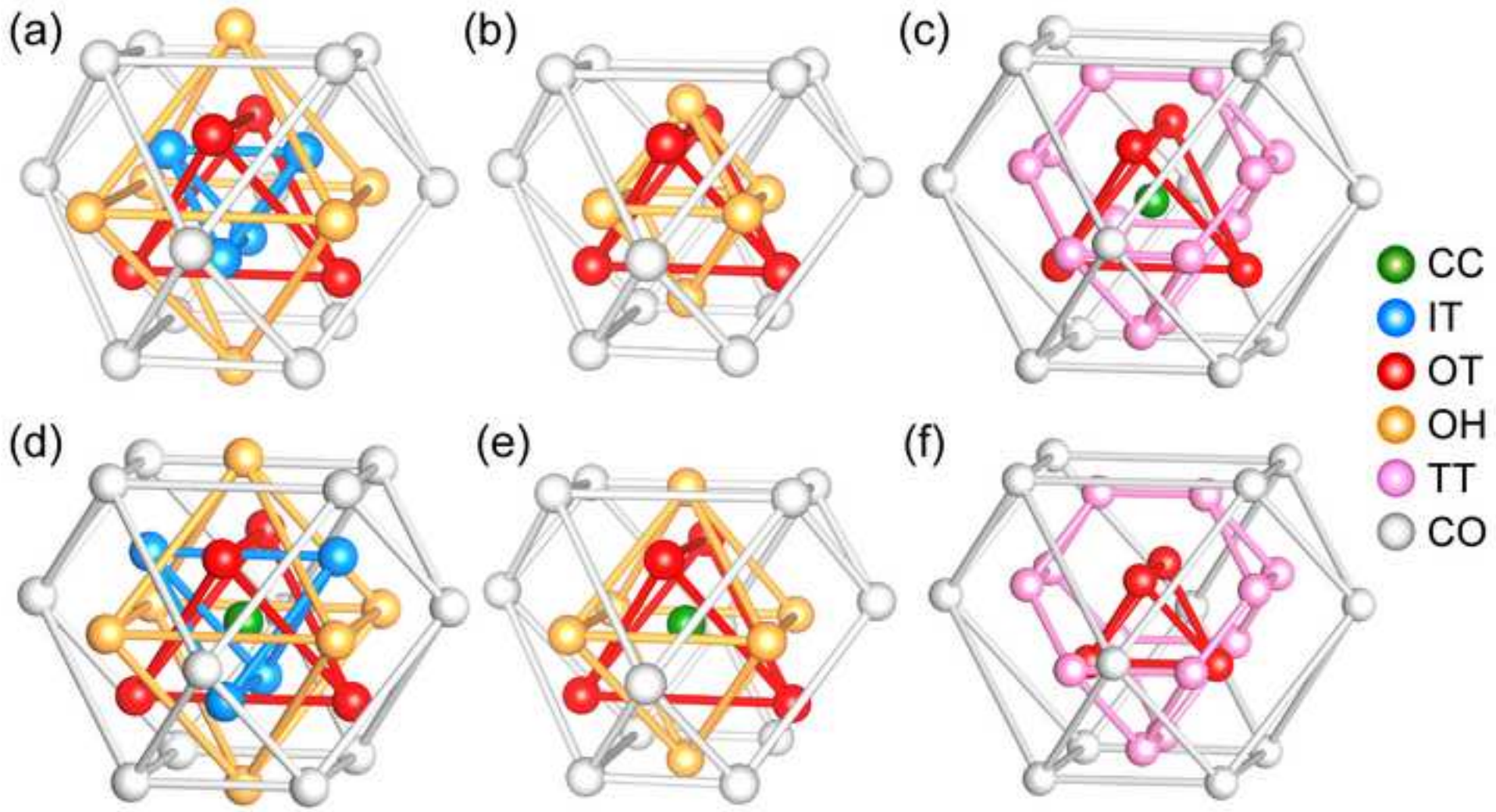

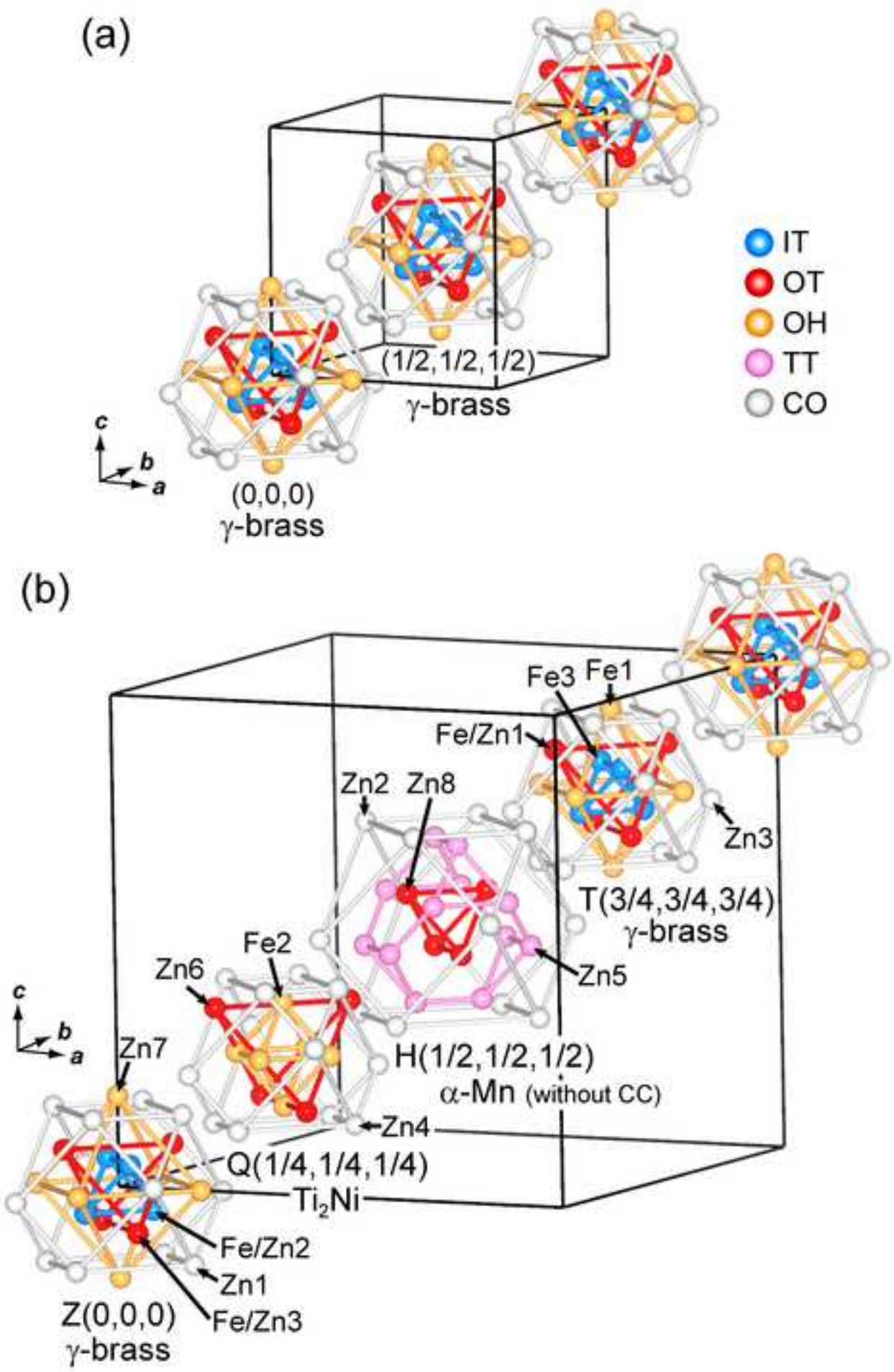

fig3.tif

Click here to download high resolution image

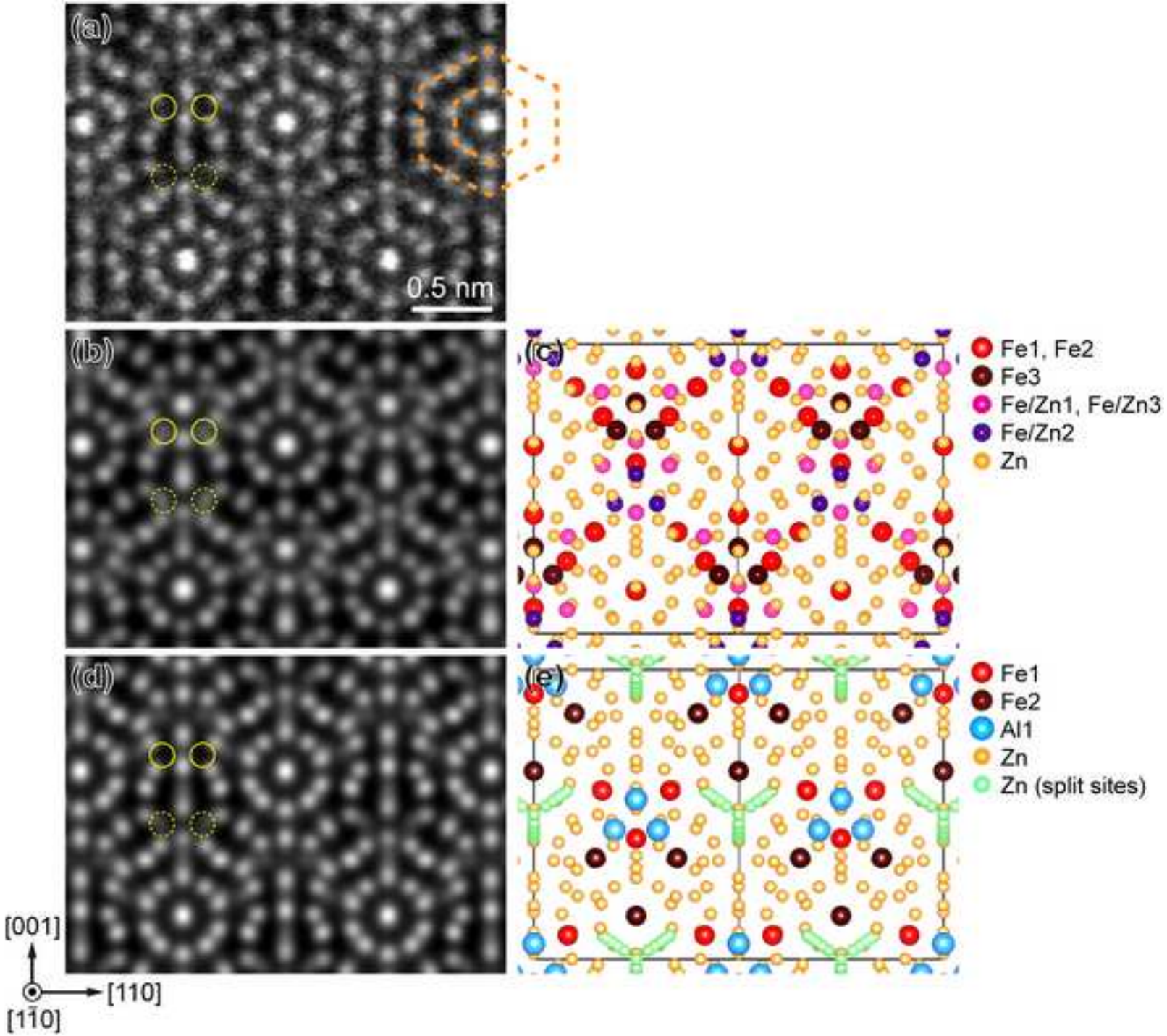

fig4.tif
Click here to download high resolution image

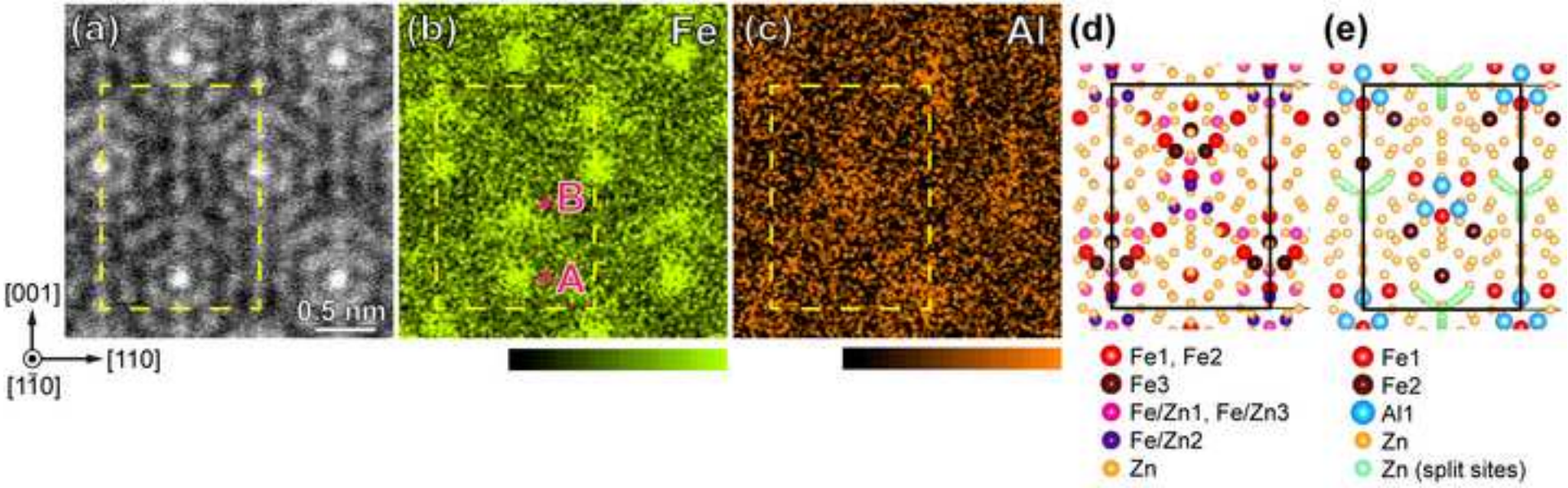

fig5.tif
Click here to download high resolution image

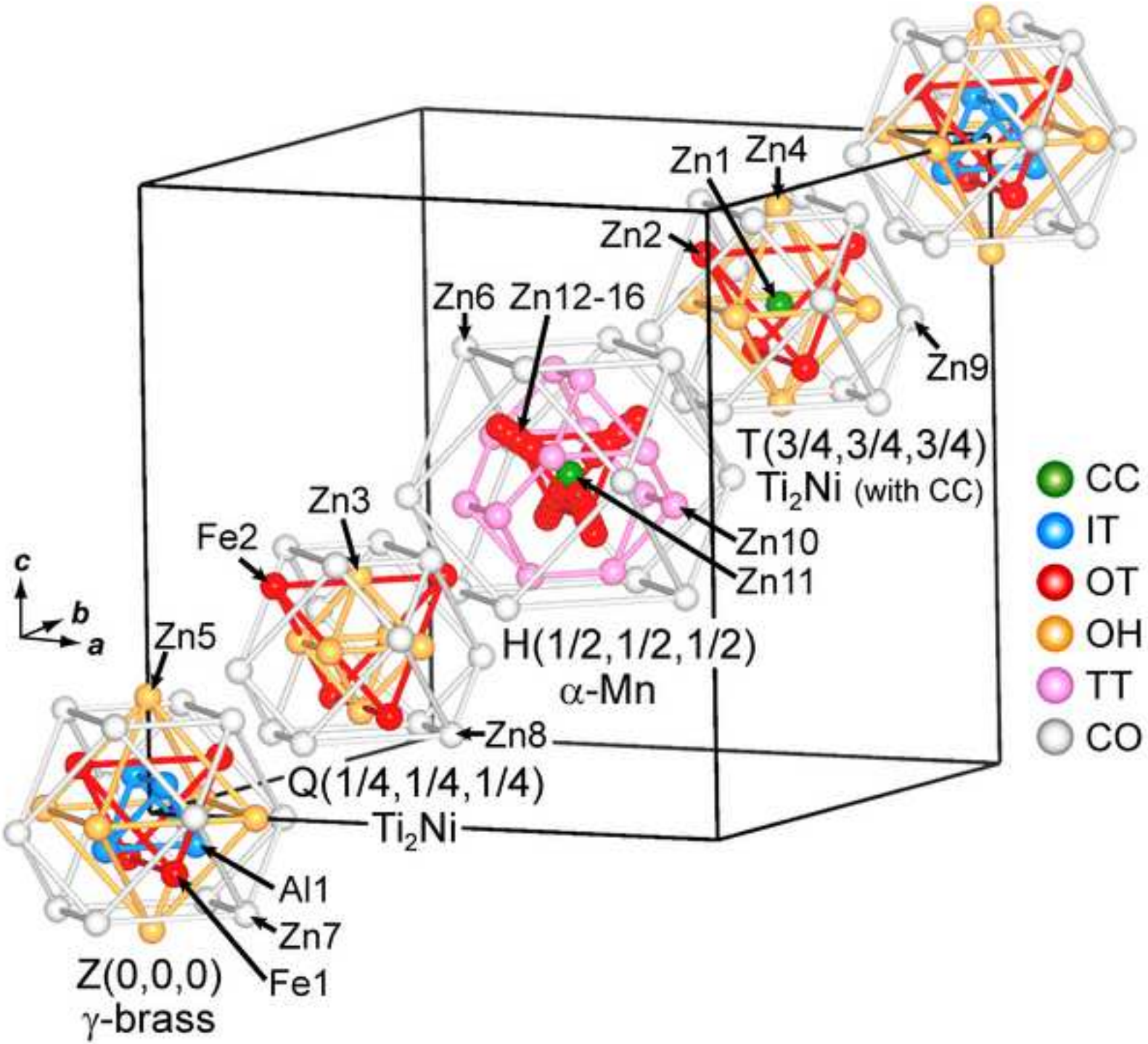

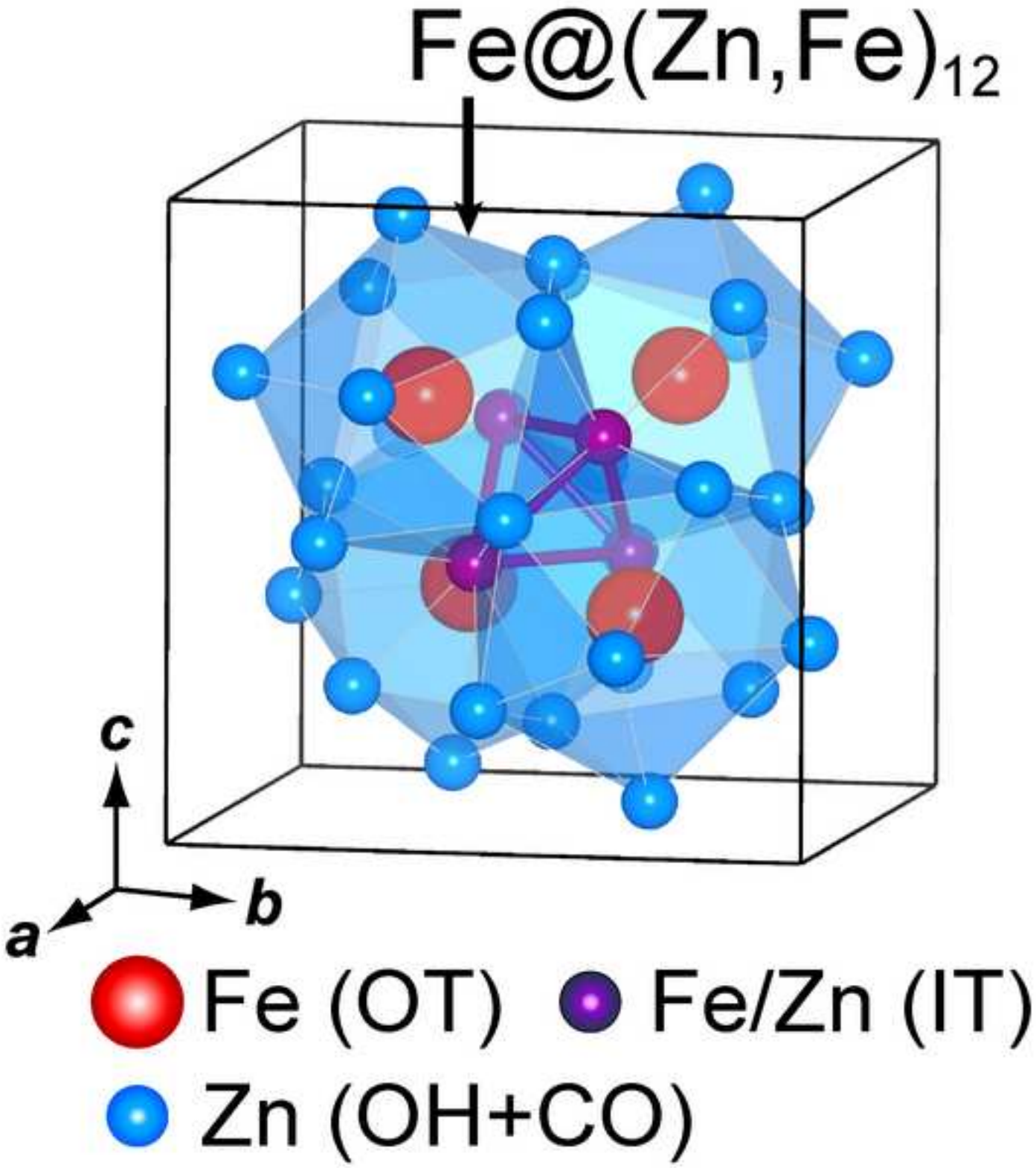

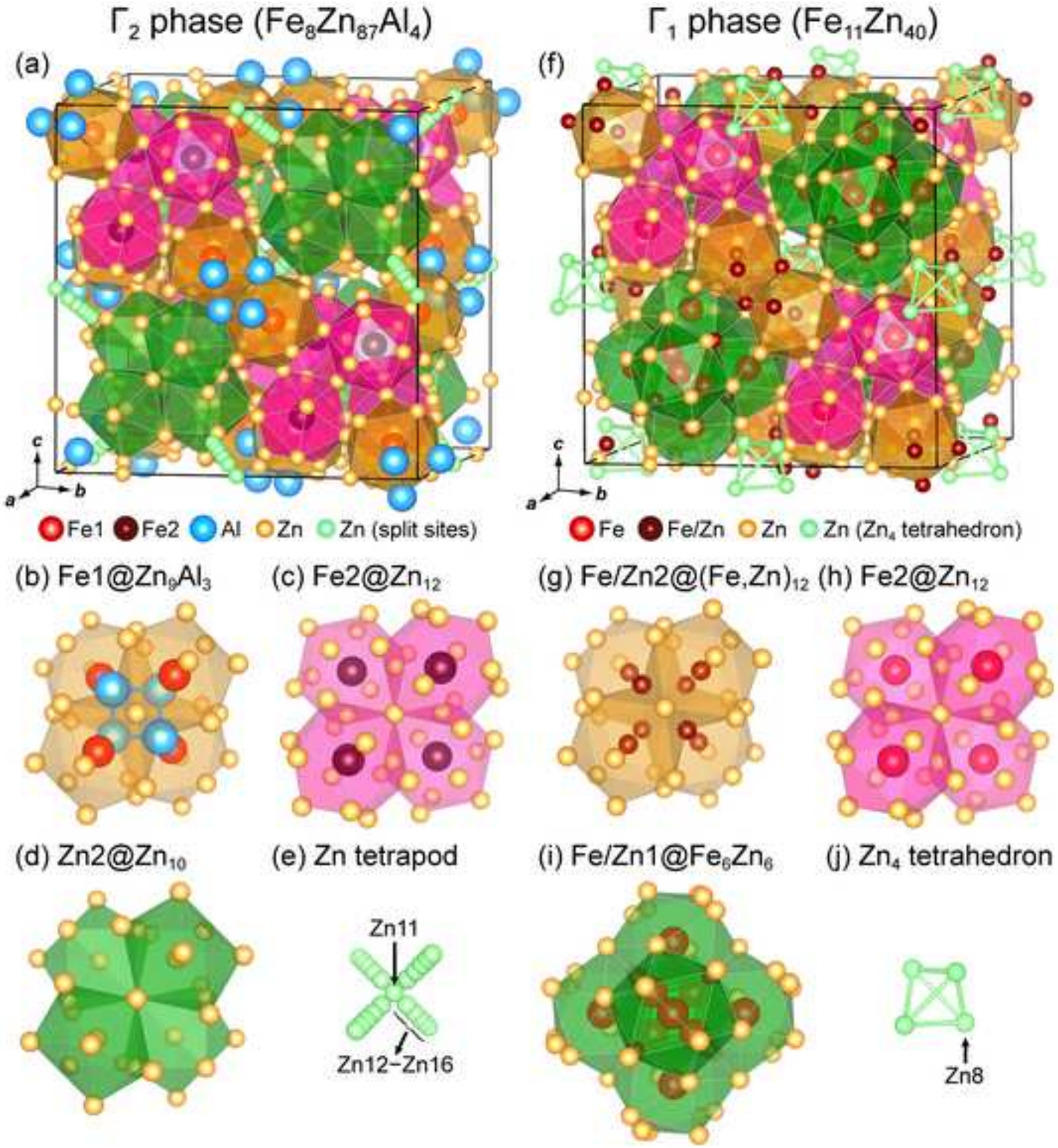

fig8.tif
Click here to download high resolution image